Effective spin models for spinor lattice gases with gauge fields

Tongyue Sun,[1] Yi Zheng,[2] Shi-jie Yang,[1] and Shuo Yang[2,3]
[1]*Department of Physics, Beijing Normal University, Beijing 100875, China*
[2]*State Key Laboratory of Low-Dimensional Quantum Physics and Department of Physics, Tsinghua University, Beijing 100084, China*
[3]*Frontier Science Center for Quantum Information, Beijing 100193, China*

(Received 7 September 2020; revised 22 December 2020; accepted 22 December 2020; published 21 January 2021)

We study the effective spin models for a Mott insulating Bose-Hubbard model in the presence of gauge fields. We first introduce a simple method based on adiabatic elimination to determine the low-energy effective Hamiltonian. Demonstration of a two-component one-dimensional model with synthetic magnetic field is shown. We further consider a generalized Bose-Hubbard model which covers the cases where spin-orbit coupling and synthetic flux are present. The resulting *XYZ* model contains Dzyaloshinskii-Moriya interactions and symmetric anisotropic couplings. Under certain conditions, this model reduces to various interesting magnetic Hamiltonians. Phase diagrams for two typical situations are obtained. We investigate magnetic phase transitions by focusing on order parameters and spin-spin correlations. Results are validated by numerical calculations using tensor network algorithms.

DOI: 10.1103/PhysRevA.103.013316

I. INTRODUCTION

Ultracold atoms in optical lattice have been proven a versatile toolbox for the study of many-body quantum systems [1,2]. Lattice gases provide a quantum simulator for Hubbard model with parameters in a wide range of regimes [3–5]. This is due to the flexibility of the choice of atomic species, as well as the high level of controllability of external fields. By addressing the laser field and manipulating Feshbach resonance [6–8], the Hubbard model can be explored from superfluid to Mott insulating phases [9–11]. Recent experiments have also reported on the realization of synthetic gauge fields [12–16], paving the way to the study of lattice gases in presence of magnetic fields and spin-orbit couplings (SOCs) [17–22]. For spinor gases in a one-dimensional (1D) optical lattice, tunable gauge fields can be engineered by Raman-assisted tunnelings [14–16], resulting in a ladder-like lattice with spins constituting the synthetic dimension.

In the deep Mott regime, charge fluctuations are suppressed at unit filling. However, for two-species spinor gases, there are nearest-neighbor tunnelings of one component followed by a backward hopping of the other component. Such a second-order process typically yields a spin-exchange interaction. The low-energy physics of the corresponding Hubbard model is captured by an effective Heisenberg model [23–25]. The presence of a synthetic gauge field such as the SOC gives rise to the well-known Dzyaloshinskii-Moriya (DM) exchange interaction [26–33], which has received much attention over the past decades [34–41]. On one hand, it appears in strongly correlated electronic materials including cuprate superconductors [34] and low-dimensional magnetic materials [41]. On the other hand, the DM interaction may induce exotic magnetic phases, such as a vortex structure and even a Skymion crystal in a two-dimensional (2D) lattice [28–30]. For the case of 1D spin chains, a SOC is characterized by spin-flip hoppings which give rise to a DM interaction in one direction. In such a case, the vortex and crystal phases may be replaced by a gapless spiral phase within the description of Luttinger liquid [32,42]. Furthermore, an artificial magnetic field characterized by synthetic flux has also been realized in cold atom experiments [12,13,15,16,18]. The presence of SOCs and an artificial magnetic field may provide an anisotropy in the Heisenberg interaction, leading to an effective spin model with spin-couplings, external fields, and DM interactions highly tunable.

To derive the effective spin model for spinor lattice gases with strong interactions, one can directly apply the second-order perturbation theory by treating the hopping terms as perturbations [24,43]. Another method is to follow the Schriffer-Wolf transformation, which combines techniques of rotation-wave approximation and high-frequency expansion. Although these methods have proven useful in the case of a strongly interacting Fermi-Hubbard model [23,44], the formalism can be quite complex, especially for spinor bosons with both interspin and intraspin interactions.

In the present paper, we first introduce an easy to implement method based on adiabatic elimination [45,46] to obtain effective spin models for lattice gases. We then investigate the effect of synthetic gauge fields on bosons with two hyperfine states in the Mott insulating regime. Spin-flip hoppings with a phase factor are considered to cover different cases of effective SOCs. We show that the corresponding effective Hamiltonian constitutes an *XYZ* model with staggered DM interactions and symmetric anisotropic couplings. Under certain conditions, this Hamiltonian reduces to various spin models. Ground state phases for some typical cases are explored.

The paper is organized as follows. In Sec. II we briefly review the idea of adiabatic elimination, based on which we

introduce a simple approach to obtain the low-energy effective Hamiltonian. In Sec. III we consider a generalized Bose-Hubbard model with SOCs and synthetic flux. The effective spin model is then obtained. The situation of an *XYZ* model with DM interaction and transverse field is studied in Sec. IV. In Sec. V we further investigate the interplay between the DM interaction and a symmetric anisotropic coupling in the *XYZ* model. A summary is included in Sec. VI.

II. LOW-ENERGY HAMILTONIAN FROM ADIABATIC ELIMINATION

Suppose that a physical system is featured by a wide energy gap or a large timescale, then the technique of adiabatic elimination can be applied to obtain an effective description that is equivalent to the low-energy physics or the slow evolution of the original system. For such a system, we consider the Schrödinger equation ($\hbar = 1$) $i\partial_t|\psi\rangle = H|\psi\rangle$ with H the full Hamiltonian acting on Hilbert space $\mathbb{H}$. We can introduce two projectors P and $Q = 1 - P$ which lead to $P|\psi\rangle \in \mathbb{H}_0$ and $Q|\psi\rangle \in \mathbb{H}_1$, with $\mathbb{H} = \mathbb{H}_0 \oplus \mathbb{H}_1$. The dynamics is governed by

$$i\partial_t \begin{pmatrix} \alpha \\ \beta \end{pmatrix} = \begin{pmatrix} \omega & \Omega^\dagger \\ \Omega & \Delta \end{pmatrix} \begin{pmatrix} \alpha \\ \beta \end{pmatrix} \tag{1}$$

with ω, Ω, and Δ the matrix forms of PHP, QHP, and QHQ, respectively. Assume that $\mathbb{H}_0$ and $\mathbb{H}_1$ are of dimensions m and n, thus α and β are $m\times 1$ and $n\times 1$ matrices representing probability amplitudes for $P|\psi\rangle$ and $Q|\psi\rangle$. In general, we consider that the eigenvalues of Δ are much larger than that of ω. If the system is initialized with a state in $\mathbb{H}_0$, excited states in $\mathbb{H}_1$ will be essentially unpopulated. Thus by simply setting $\partial_t\beta = 0$, we obtain the effective evolution equation for states in $\mathbb{H}_0$, which yields the low-energy Hamiltonian [46–48]

$$H_{\text{eff}} = \omega - \Omega^\dagger \Delta^{-1} \Omega. \tag{2}$$

To demonstrate the application of this formalism in the Hubbard model, we first consider two-species bosons in a 1D optical lattice, as described by

$$\hat{H} = -\sum_{j,\sigma} (t_\sigma e^{-i\eta_\sigma \phi} \hat{a}^\dagger_{j,\sigma} \hat{a}_{j+1,\sigma} + \text{H.c.}) - \frac{t'}{2} \sum_{j,\sigma} \hat{a}^\dagger_{j,\bar{\sigma}} \hat{a}_{j,\sigma} + \sum_j U_{\uparrow\downarrow} \hat{n}_{j,\uparrow} \hat{n}_{j,\downarrow} + \frac{1}{2} \sum_{j,\sigma} U_\sigma \hat{n}_{j,\sigma} (\hat{n}_{j,\sigma} - 1). \tag{3}$$

Here $\sigma \in \{\uparrow, \downarrow\}$ labels the quasispin. $\bar{\sigma} = \downarrow$ ($\uparrow$) and $\eta_\sigma = 1$ (-1) for $\sigma = \uparrow$ ($\downarrow$). The number operator is defined by $\hat{n}_{j,\sigma} = \hat{a}^\dagger_{j,\sigma} \hat{a}_{j,\sigma}$. $\hat{a}_{j,\sigma}$ denotes the bosonic annihilation operator for spin σ acting on site j. A schematic diagram of the model is exhibited in Fig. 1(a). The first term of Eq. (3) describes a nearest-neighbor hopping for spin-σ with tunneling amplitude t_σ. An artificial magnetic field is captured by a synthetic flux (2ϕ per plaquette). $t'/2$ denotes the spin-flip amplitude. $U_{\uparrow\downarrow}$ and U_σ are interspin and intraspin interactions. Here we set $U_{\uparrow\downarrow}, U_\sigma \gg t_\sigma, t'$ in order to map the Hamiltonian to a spin model.

We consider a dimer system at unit filling, then the matrices in Eq. (1) can be obtained straightforwardly. Without spin-flip processes ($t' = 0$), we simply have $\omega = 0$ and $\Delta = \text{diag}(U_{\uparrow\downarrow}, U_{\uparrow\downarrow}, U_\uparrow, U_\uparrow, U_\downarrow, U_\downarrow)$. Ω is given by

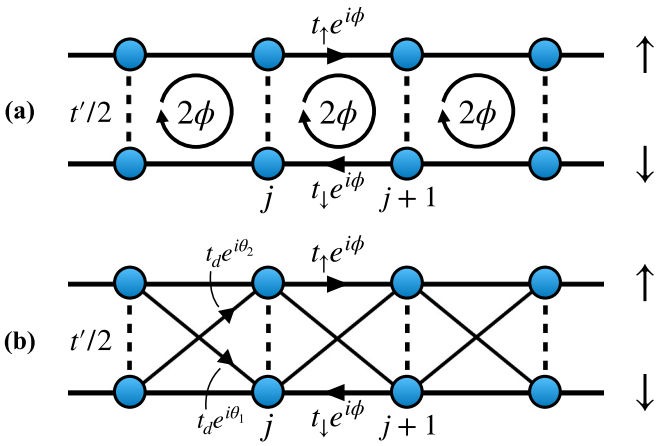

FIG. 1. Schematic diagram of lattice models described by (a) Eq. (3) and (b) Eq. (7). The two legs labeled by ↑ and ↓ indicate pseudospins of the lattice gas.

$$\begin{array}{c|cccc|c} & \uparrow,\uparrow & \uparrow,\downarrow & \downarrow,\uparrow & \downarrow,\downarrow & \\ \hline & & -t_\downarrow e^{i\phi} & -t_\uparrow e^{-i\phi} & & \uparrow\downarrow, 0 \\ & & -t_\uparrow e^{i\phi} & -t_\downarrow e^{-i\phi} & & 0, \uparrow\downarrow \\ -\sqrt{2}t_\uparrow e^{-i\phi} & & & & & \uparrow\uparrow, 0 \\ -\sqrt{2}t_\uparrow e^{i\phi} & & & & & 0, \uparrow\uparrow \\ & & & & -\sqrt{2}t_\downarrow e^{i\phi} & \downarrow\downarrow, 0 \\ & & & & -\sqrt{2}t_\downarrow e^{-i\phi} & 0, \downarrow\downarrow \end{array}.$$

Here the corresponding basis vectors are labeled on the top and right. Specifically, the matrix elements of Ω correspond to $\langle d|H_{\text{dimer}}|p\rangle$ with basis vectors $|p\rangle \in \{|\uparrow,\uparrow\rangle, \ |\uparrow,\downarrow\rangle, \ |\downarrow,\uparrow\rangle, \ |\downarrow,\downarrow\rangle\}$ and $|d\rangle \in \{|\uparrow\downarrow, 0\rangle, \ |0,\uparrow\downarrow\rangle, \ |\uparrow\uparrow, 0\rangle, \ |0,\uparrow\uparrow\rangle, \ |\downarrow\downarrow, 0\rangle, \ |0,\downarrow\downarrow\rangle\}$. For example, $\Omega_{1,2} = \langle\uparrow\downarrow, 0|H_{\text{dimmer}}|\uparrow,\downarrow\rangle = -t_\downarrow e^{i\phi}$. We have used the notation $|\uparrow,\downarrow\rangle = \hat{a}^\dagger_{1,\uparrow}\hat{a}^\dagger_{2,\downarrow}|0,0\rangle$ for a pair state and $|\uparrow\downarrow, 0\rangle = \hat{a}^\dagger_{1,\uparrow}\hat{a}^\dagger_{1,\downarrow}|0,0\rangle$ for a doublon state. Now with Eq. (2) we have

$$H_{\text{eff}} = -\begin{bmatrix} \uparrow,\uparrow & \uparrow,\downarrow & \downarrow,\uparrow & \downarrow,\downarrow & \\ \hline \frac{4t_\uparrow^2}{U_\uparrow} & & & & \uparrow,\uparrow \\ & \frac{t_\uparrow^2+t_\downarrow^2}{U_{\uparrow\downarrow}} & \frac{2t_\uparrow t_\downarrow e^{-2i\phi}}{U_{\uparrow\downarrow}} & & \uparrow,\downarrow \\ & \frac{2t_\uparrow t_\downarrow e^{2i\phi}}{U_{\uparrow\downarrow}} & \frac{t_\uparrow^2+t_\downarrow^2}{U_{\uparrow\downarrow}} & & \downarrow,\uparrow \\ & & & \frac{4t_\downarrow^2}{U_\downarrow} & \downarrow,\downarrow \end{bmatrix}. \tag{4}$$

For more complicated models, the calculation can be carried out conveniently with a few lines of Python code based on SymPy [49]. Defining the spin operators $\vec{S}_j = \frac{1}{2}\psi_j^\dagger \vec{\sigma} \psi_j$ with $\psi_j^\dagger = (\hat{a}^\dagger_{j,\uparrow}, \hat{a}^\dagger_{j,\downarrow})$ and $\vec{\sigma} = (\sigma_x, \sigma_y, \sigma_z)$, Eq. (4) is mapped to a two-site spin model. This can be done by comparing Eq. (4) with $H_s = \sum_{a,b} J_{a,b} \cdot S_1^a \otimes S_2^b + \sum_a h_a (S_1^a \otimes \hat{1} + \hat{1} \otimes S_2^a) + \Delta E \cdot \hat{1} \otimes \hat{1}$. Here ΔE, $J_{a,b}$, and h_a (with $a, b \in \{x, y, z\}$) are regarded as coefficients to be determined. Extending the obtained model to a lattice then yields

$$H_s = \sum_j \left[\sum_a J_a S_j^a S_{j+1}^a + \vec{D} \cdot (\vec{S}_j \times \vec{S}_{j+1}) + h_z S_j^z \right]. \tag{5}$$

The parameters are given by

$$\begin{aligned} J_x &= J_y = -4t_\uparrow t_\downarrow \cos(2\phi)/U_{\uparrow\downarrow}, \\ J_z &= -4t_\uparrow^2/U_\uparrow - 4t_\downarrow/U_\downarrow + 2\big(t_\uparrow^2 + t_\downarrow^2\big)/U_{\uparrow\downarrow}, \\ \vec{D} &= 4t_\uparrow t_\downarrow \sin(2\phi)\hat{z}/U_{\uparrow\downarrow}, \\ h_z &= 2t_\uparrow^2/U_\uparrow - 2t_\downarrow^2/U_\downarrow. \end{aligned} \tag{6}$$

We have ignored a trivial energy shift $\Delta E = -[t_\uparrow^2/U_\uparrow + t_\downarrow^2/U_\downarrow + (t_\uparrow^2 + t_\downarrow^2)/(2U_{\uparrow\downarrow})](L-1)$ with L the lattice size. The effective Hamiltonian describes an XXZ model with z-component DM interaction as well as a longitudinal field. For $t' \neq 0$, the interspin hopping in a dimer system leads to $\omega = -t'(S^x \otimes \hat{1} + \hat{1} \otimes S^x)$, which yields an additional transverse-field term $-t' \sum_j S_j^x$ to Eq. (5). We mention that without the interspin coupling, the ladder in Fig. 1(a) becomes two independent chains and the synthetic flux can be gauged away (through the transformation $\hat{a}_{j,\sigma} \to e^{i\eta_\sigma \phi j}\hat{a}_{j,\sigma}$). As a result, Eq. (5) reduces to an XXZ model without DM interaction [50].

III. EFFECTIVE SPIN MODEL FOR BHM WITH GAUGE FIELDS

We take the spin-flip tunnelings into account. For simplicity, we assume $t_\uparrow = t_\downarrow = t\cos\alpha$ and the spin-flip hopping rate is $t\sin\alpha$. The hopping terms are given by

$$\begin{aligned} \hat{H} = &-t\cos\alpha \sum_j (e^{-i\phi}\hat{a}_{j,\uparrow}^\dagger \hat{a}_{j+1,\uparrow} + e^{i\phi}\hat{a}_{j,\downarrow}^\dagger \hat{a}_{j+1,\downarrow}) \\ &- t\sin\alpha \sum_j (e^{-i\theta_1}\hat{a}_{j,\uparrow}^\dagger \hat{a}_{j+1,\downarrow} + e^{-i\theta_2}\hat{a}_{j,\downarrow}^\dagger \hat{a}_{j+1,\uparrow}) \\ &- \frac{t'}{2}\sum_j \hat{a}_{j,\uparrow}^\dagger \hat{a}_{j,\downarrow} + \text{H.c.} \end{aligned} \tag{7}$$

The schematic diagram of this lattice model is shown in Fig. 1(b). Without hopping phases, the Hamiltonian constitutes a Creutz ladder by regarding the spins as a synthetic spacial dimension. Such a Creutz ladder has been created in atomic systems and circuit QED [51–53]. The phase ϕ (along the legs) indicates a synthetic magnetic flux within a plaquette. We have also introduced two hopping phases θ_1 and θ_2 to cover typical cases of SOCs. For example, a SOC of the form $p_x\sigma_y$ (an equal-weight combination of the Rashba and Dresselhause couplings) corresponds to $\theta_1 = \pi$ and $\theta_2 = 0$. The Hamiltonian can be rewritten as $H = -t\sum_{\langle jl\rangle} \hat{\psi}_j^\dagger \mathcal{R}_{jl}\hat{\psi}_l$, with $\mathcal{R}_{jl} = \exp[i\alpha(l-j)\sigma_y]$ and $\hat{\psi}_j^\dagger = (\hat{a}_{j,\uparrow}^\dagger, \hat{a}_{j,\downarrow}^\dagger)$. Analogously for a SOC of the form $p_x\sigma_x$, we have $\mathcal{R}_{jl} = \exp[i\alpha(l-j)\sigma_x]$ corresponding to $\theta_1 = \theta_2 = -\pi/2$. Here we give general results based on Eq. (7). We note that both the synthetic flux and the Rashba-Dresselhause SOC can be implemented for ultracold atoms in an optical lattice [15–19], thus we focus our discussion on such situations in following sections.

At unit filling, we take into account the interactions in Eq. (3) with $U_\uparrow = U_\downarrow = U$ and $U_{\uparrow\downarrow} = \lambda U$. Under the condition $U \gg t, t'$, we follow the adiabatic elimination in Sec. II and obtain the low-energy effective Hamiltonian:

$$\begin{aligned} H_s = &\sum_{j,a} \big[J_a S_j^a S_{j+1}^a + \Gamma_a\big(S_j^b S_{j+1}^c + S_j^c S_{j+1}^b\big)\big] \\ &+ \sum_j \big[\vec{D}\cdot(\vec{S}_j \times \vec{S}_{j+1}) + h_x S_j^x + h_y S_j^y\big]. \end{aligned} \tag{8}$$

Here $a \in \{x, y, z\}$, b, and c indicate the two remaining directions besides a. The second term refers to symmetric anisotropic exchange [26,27] and has been studied in the context of honeycomb iridates [54]. The spin exchange interaction strengths in the first term are given by

$$\begin{aligned} J_x &= -\frac{4t^2}{\lambda U}[\cos^2(\alpha)\cos(2\phi) + \sin^2(\alpha)\cos(\theta_1 - \theta_2)], \\ J_y &= -\frac{4t^2}{\lambda U}[\cos^2(\alpha)\cos(2\phi) - \sin^2(\alpha)\cos(\theta_1 - \theta_2)], \\ J_z &= -\frac{4t^2}{\lambda U}[\cos(2\alpha)(2\lambda - 1)]. \end{aligned} \tag{9}$$

Other parameters are given in Table I. Equation (8) constitutes a very general spin model controlled by parameters λ, α, and $\theta_{1(2)}$. By tuning these parameters, various spin models can be realized. In the following sections, we discuss two typical cases.

Before proceeding, we can check the result with a symmetry analysis. For $\phi = 0$, the Hamiltonian in Eq. (7) is invariant under a real-space mirror reflection ($M: j \to -j$) followed by a time-reversal operation ($R = K\sigma_x$). Here the time reversal refers to complex conjugation together with spin reversal. As for the effective Hamiltonian, the Γ terms are symmetric under the mirror reflection, whereas the DM coupling terms are antisymmetric under M. It can be then verified that the spin couplings (corresponding to nonzero coefficients D_x, D_y, and Γ_z) possess the same symmetry (the operation of RM). Analogously, for $\theta_1 = -\theta_2$ and $\phi \neq 0$, both the original Hamiltonian and the effective spin model (including terms of D_z and Γ_z) are time reversal symmetric. Furthermore, for $\theta_1 = -\theta_2$ and $\phi = 0$ or π, Γ_z term is remained. This is in accordance with the mirror symmetry in Eq. (7).

IV. XYZ MODEL WITH DM COUPLING AND TRANSVERSE FIELD

We first consider a simplified case where the symmetric anisotropic coupling is excluded. This can be achieved by setting $\phi = \theta_2 = 0$ and $\theta_1 = \pi$ as in the case of Rashba-Dresselhause SOCs. The corresponding spin model is given by

$$\begin{aligned} H_1 = -\frac{1}{\lambda}\sum_j \big[&\cos(2\alpha)S_j^x S_{j+1}^x + \cos(2\alpha)(2\lambda - 1)S_j^y S_{j+1}^y \\ &+ S_j^z S_{j+1}^z + \lambda\sin(2\alpha)\big(S_j^x S_{j+1}^y - S_j^y S_{j+1}^x\big)\big] \\ &- h_x \sum_j S_j^x. \end{aligned} \tag{10}$$

Note that we have made a rotation around $\hat{x}$ by an angle $\pi/2$ ($\hat{y} \to \hat{z}$, $\hat{z} \to -\hat{y}$) so that the DM vector is along the $\hat{z}$ axis. $h_x = t'/J$ and hereafter we set $J \equiv 4t^2/U$ as the unit of

TABLE I. Parameters for the effective Hamiltonian (8).

$D_x = \frac{2t^2}{U}\sin(2\alpha)\cos\phi[\sin(\theta_1)+\sin(\theta_2)]$	$\Gamma_x = -\frac{2t^2}{U}\sin(2\alpha)\sin(\phi)[\cos(\theta_1)-\cos(\theta_2)]$
$D_y = \frac{2t^2}{U}\sin(2\alpha)\cos\phi[\cos(\theta_1)-\cos(\theta_2)]$	$\Gamma_y = -\frac{2t^2}{U}\sin(2\alpha)\sin(\phi)[\sin(\theta_1)+\sin(\theta_2)]$
$D_z = \frac{4t^2}{\lambda U}\cos^2(\alpha)\sin(2\phi)$	$\Gamma_z = \frac{4t^2}{\lambda U}\sin^2(\alpha)\sin(\theta_1-\theta_2)$
$h_x = -\frac{2t^2(\lambda+1)}{\lambda U}\sin(2\alpha)\cos(\phi)[\cos(\theta_1)+\cos(\theta_2)]-t'$	$h_y = \frac{2t^2(\lambda+1)}{\lambda U}\sin(2\alpha)\cos(\phi)[\sin(\theta_1)-\sin(\theta_2)]$

energy. In general, we can restrict our discussion in the regime $\alpha \in [0, \pi/2]$. Without a magnetic field, the *XYZ* model with z-component DM interaction has been well studied [30–32,39]. For $\lambda < 1$, the ferromagnetic phase along $\hat{z}$ (z-FM) is favored since $S^z_j S^z_{j+1}$ is the leading coupling term, whereas for $\lambda > 1$, the dominate terms are DM interaction and spin-spin coupling along $\hat{e}_y$. Thus at small α one may expect a ferromagnetic phase along the $\hat{y}$ direction (y-FM). For $\alpha \sim \pi/4$, the DM interaction plays an essential role, leading to a spiral phase in $\hat{x}$-$\hat{y}$ plane (xy-SP). For $\alpha \sim \pi/2$, J_y of the dominant S^y-S^y coupling is positive, corresponding to an antiferromagnetic phase along $\hat{y}$ (y-AF). On the other hand, the transverse field may induce transitions from the above phases to a paramagnetic phase (x-PM).

To characterize these phases, we take the order parameters: magnetization $M_a = 1/L|\sum_j \langle S^a_j\rangle|$ with $a = x, y, z$, staggered magnetization $N_a = 1/L|\sum_j (-1)^j \langle S^a_j\rangle|$, as well as the spiral order $C_a = 1/(L-1)|\sum_j \langle \hat{a}\cdot(\vec{S}_j \times \vec{S}_{j+1})\rangle|$, with L the lattice size. These quantities are numerically calculated using time evolving block decimation (TEBD) [55–57]. The phase diagram as a function of α and h_x for $\lambda = 1.2$ is shown in Fig. 2, which is in agreement with the above arguments. The appearance of y-FM, y-AF, xy-SP, and x-PM are featured by nonzero M_y, N_y, C_z, and M_x, respectively.

Order parameters versus α for $h_x = 0.2$ (along the vertical dashed line) are depicted in Fig. 3(a), with the increase of α, the competition between DM interaction and spin-spin coupling in the $\hat{y}$ direction leads to the y-FM-xy-SP-y-AF transitions. We observe nearly saturated magnetization and staggered magnetization in y-FM and y-AF. At transition points $\alpha_c \simeq (0.076 \pm 0.001)\pi$ and $\alpha_c \simeq (0.426 \pm 0.001)\pi$, there are cliffs, respectively, for M_y and N_y, signaling first-order phase transitions. The appearance of xy-SP can be implied by setting $h_x = 0$ and $\alpha = \pi/4$. In such a situation, Eq. (10) reduces to

$$H_1^{\pi/4} = -\sum_j \left[\frac{1}{\lambda} S^z_j S^z_{j+1} + \left(S^x_j S^y_{j+1} - S^y_j S^x_{j+1}\right)\right] \quad (11)$$

and can be mapped onto a well-known *XXZ* model through a rotation ($j\pi/2$ around $\hat{z}$) of each local spin. The resulting *XXZ* model possesses a gapless *XY* phase [58], which indicates a four-site-period spiral order for the original model [32,59]. With a small transverse field, such a phase translates to a spiral phase with period deviated from four [33]. When α is close to $\pi/4$, the DM term still dominates and this picture remains valid. By increasing the transverse field, as shown in Fig. 3(b) for $\alpha = 0.4\pi$ (along the horizontal line in Fig. 2), the system undergoes an xy-SP-y-AF phase transition and eventually enters the x-PM phase. M_x is finite in all phases due to the presence of transverse field, but other order parameters are zero in the x-PM. The y-AF-x-PM phase transition can be inferred from the situation of $\alpha = \pi/2$. In this limit, Eq. (10) reduces to an *XYZ* model with transverse field. In such a case, the antiferromagnetic to paramagnetic phase transition is continuous and is in the universality class of an Ising model in a transverse field [60]. As α deviates from $\pi/2$, the y-AF does not vanish immediately, and we expect that the transition to x-PM will not change qualitatively.

Furthermore, these phases can also be characterized by correlation function $\langle S^a_i S^a_j\rangle$ ($a = x, y, z$) and structure factor $\mathcal{S}^a(q) = \langle \sum_{i,j} e^{iq(i-j)} S^a_i S^a_j\rangle/L$. To perform numerical simulations, a method called variational Matrix-Product-State (vMPS) is adopted, which is based on tensor network algorithms and is equivalent to the density matrix renormalization group [57,61,62]. In Fig. 4 we demonstrate correlation functions (a1–a3) and structure factors (b1–b3) at representative points labeled in Fig. 2. The parameters are $h_x = 0.2,\ 1.0,\ 1.2$ (with $\alpha = 0.4\pi$), corresponding to xy-SP, y-AF, and x-PM, respectively. In Fig. 4(a1) $\langle S^x_i S^x_j\rangle$ and $\langle S^y_i S^y_j\rangle$ show oscillations without decaying even in the long range. Such behaviors can be seen from the peaks of $\mathcal{S}_x$ and $\mathcal{S}_y$. As shown in Fig. 4(b1), there are clear peaks at $q_{x(y)} = Q_{x(y)} \simeq 0.826\pi$.

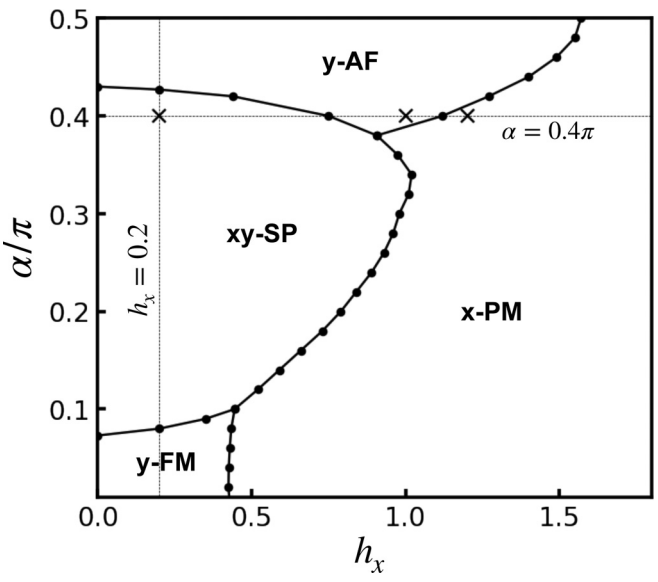

FIG. 2. Phase diagram of the Hamiltonian (10) spanned by α and h_x. We have set $\lambda = 1.2$. With a small transverse field, there are ferromagnetic and antiferromagnetic phases along the $\hat{y}$ direction. The xy-SP rises as a result of dominant DM interaction. The transverse field leads to a paramagnetic phase. Variations of order parameters along the vertical ($h_x = 0.2$) and horizontal ($\alpha = 0.4\pi$) lines are demonstrated in Fig. 2. The points located by crosses are analyzed in Fig. 4.

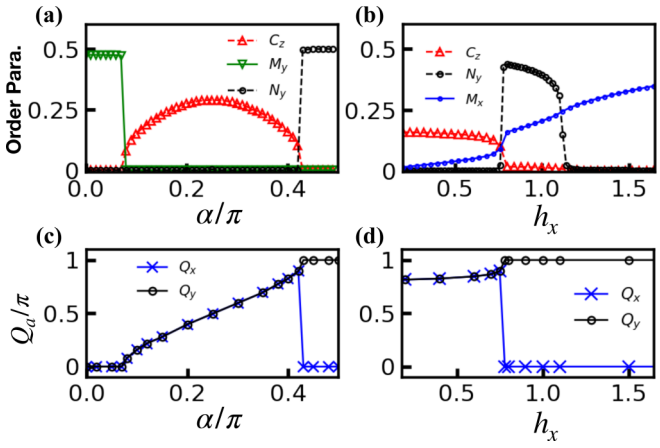

FIG. 3. Phase transitions indicated by the variation of order parameters. (a) M_y, N_y, and C_z as a function of α for $h_x = 0.2$ (along the vertical line in Fig. 2). (b) M_x, N_y, and C_z as a function of the transverse field h_x for $\alpha = 0.4\pi$ (along the horizontal line in Fig. 2). C_x and C_y (not shown) are nearly zero in all parameter regimes. (c) Characteristic wave vectors Q_x and Q_y versus α. The critical points where $Q_{x,(y)}$ deviate from 0 and π are in agreement with the transition points in (a). (d) Q_x and Q_y versus h_x. The critical point indicates the xy-SP-y-AF transition. Q_x and Q_y are calculated by locating the maxima of structure factors $\mathcal{S}_x(q)$ and $\mathcal{S}_y(q)$. The transition to x-PM is not shown by $Q_{x(y)}$, instead, it can by characterized by correlation functions and structure factors as demonstrated in Fig. 4.

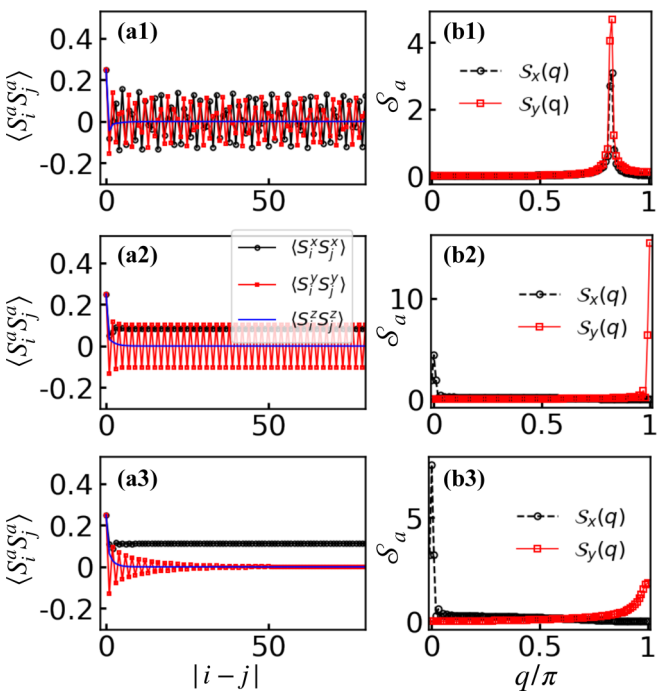

FIG. 4. Spin-spin correlation functions $\langle S_i^a S_j^a \rangle$ ($a = x, y, z$) and the structure factors $\mathcal{S}^a(q)$ obtained by vMPS calculations with lattice size $L = 200$ (open boundary). The parameters are (a1, b1) $h_x = 0.2$ (in the xy-SP), (a2, b2) $h_x = 1.0$ (in the y-AF), and (a3, b3) $h_x = 1.2$ (in the x-PM) as labeled in Fig. 2. (a1–a3) $\langle S_i^a S_j^a \rangle$ versus $|i-j|$ in different phases. (b1–b3) The corresponding structure factors $\mathcal{S}^a(q)$ as a function of wave vector q. Note that there is no long-range correlation in the $\hat{z}$ direction, thus $\mathcal{S}_z$ (not shown) has no peak and is close to zero.

Therefore, we can fit correlation functions $\langle S_i^x S_j^x \rangle$ and $\langle S_i^y S_j^y \rangle$ by $A\cos(Q_{x(y)}|i-j|+\varphi)/|i-j|^\gamma$ with A, φ, and γ fitting parameters. The characteristic wave vectors Q_x and Q_y change with parameters, but we have $0 < Q_x = Q_y < \pi$ in the xy-SP. In the y-FM [see Figs. 4(a2) and 4(b2)], $\langle S_i^y S_j^y \rangle$ shows long-range antiferromagnetic structure, as confirmed by the sharp peak of $\mathcal{S}_y$ at $Q_y = \pi$. A finite ferromagnetic correlation along $\hat{x}$ exists due to the transverse field, indicating a small peak of $\mathcal{S}_x$ at $Q_x = 0$. In the x-PM, as shown in Figs. 4(a3) and 4(b3), $\langle S_i^y S_j^y \rangle$ decays exponentially and the peak at $Q_x = \pi$ is depressed and broadened significantly. As a comparison to the phase transitions indicated by Figs. 3(a) and 3(b), we plot the characteristic wave vector $Q_{x(y)}$ as functions of α and h_x in Figs. 3(c) and 3(d). We find clear transition point at the boundary between y-FM (y-AF) and xy-SP. The y-AF-xy-SP transition is not revealed by $Q_{x(y)}$, but is characterized by the disappearance of long-range order in the $\hat{y}$ direction.

V. *XYZ* MODEL WITH DM AND SYMMETRIC ANISOTROPIC COUPLINGS

With $\theta_1 = \pi$, $\theta_2 = 0$ and $\phi \neq 0$, Eq. (7) yields a BHM with both SOCs and synthetic flux. The symmetric anisotropic interaction appears in the effective spin model, and we can study its influence on the ground state phases. Specifically, the nonzero parameters in Table I are (scaled by the energy unit $4t^2/U$):

$$\begin{aligned} \Gamma_x &= \sin(2\alpha)\sin(\phi), \\ D_y &= -\sin(2\alpha)\cos(\phi), \\ D_z &= 1/\lambda\cos^2(\alpha)\sin(2\phi). \end{aligned} \tag{12}$$

With J_a given in Eq. (6) and $D_x = 0$, the Hamiltonian is written as

$$\begin{aligned} H_2 = \sum_j \left[\sum_a J_a S_j^a S_{j+1}^a + \Gamma_x \left(S_j^y S_{j+1}^z + S_j^z S_{j+1}^y \right) \right] \\ + \sum_j \vec{D} \cdot (\vec{S}_j \times \vec{S}_{j+1}). \end{aligned} \tag{13}$$

We have neglected the transverse field for simplicity. The effect of the Γ_x term can be qualitatively understood by considering a Hamiltonian $H = \Gamma_x \sum_j (S_j^y S_{j+1}^z + S_j^z S_{j+1}^y)$. Assume $\Gamma_x > 0$, the ground state is fourfold degenerate: two ferromagnetic states along $(\hat{e}_y - \hat{e}_z)$ and two antiferromagnetic states along $(\hat{e}_y + \hat{e}_z)$. With the influence of other spin-spin couplings, the orientation may deviate in the ferromagnetic or antiferromagnetic phases, but the spins are always aligned in the $\hat{y}$-$\hat{z}$ plane. The DM term $\sum_j \vec{D} \cdot (\vec{S}_j \times \vec{S}_{j+1})$ is responsible for the chiral nature in the SP. In such a phase, both C_z and C_y can be nonzero, indicating that the spins are spiral in $\hat{x}$-$\hat{y}$ and $\hat{x}$-$\hat{z}$ planes. Thus we can take $C_y + C_z$ as the order parameter.

The phase diagram in Fig. 5 shows three phases: the SP characterized by finite $C_y + C_z$, the yz-FM with ferromagnetic orders in $\hat{y}$ and $\hat{z}$ directions, as well as the yz-AF with antiferromagnetic orders. For $\phi = 0$, this model reduces to Eq. (10) upon a rotation around $\hat{x}$, thus the FM-SP-AF transitions are in accordance with the ones in Fig. 2 along $h_x = 0$. For $\phi \sim \pi/2$,

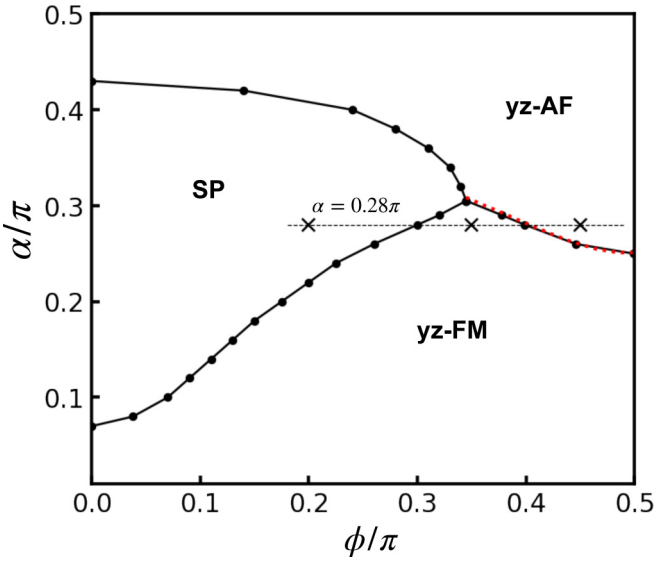

FIG. 5. Ground state phase diagram of the Hamiltonian (13). We have set $\lambda = 1.2$. The interplay between DM interactions and the Γ_x term leads to three phases as labeled in the diagram. The boundary between yz-FM and yz-AF overlaps with the curve for $J_y + J_z = 0$ (red dotted line). The crosses locate the points which are analyzed in Fig. 7.

the Γ_x term is dominant, we expect the ground state to be in the ferromagnetic or antiferromagnetic phase in the $\hat{y}$-$\hat{z}$ plane. We find that the yz-FM-yz-AF phase boundary overlaps with the curve for $J_y + J_z = 0$ (red dotted line). This indicates that the appearance of either yz-FM or yz-AF is further determined by the sign of $J_y + J_z$. In Fig. 6(a) we plot the variations of order parameters along the dashed line $\alpha = 0.28\pi$. Phase transitions are indicated by sudden changes of the spiral order,

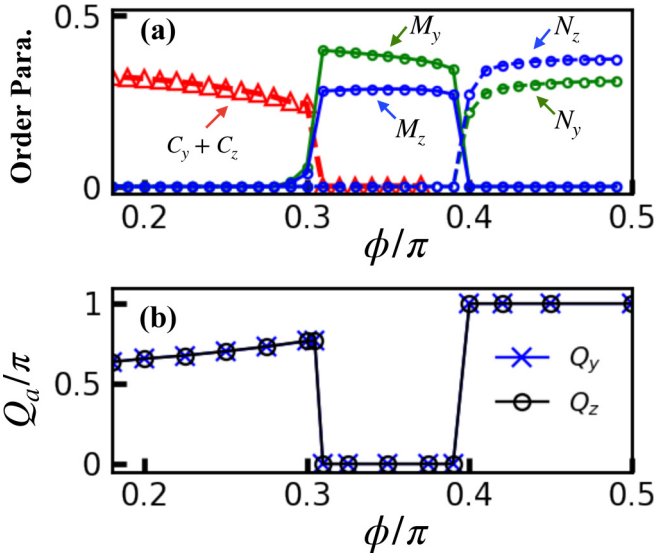

FIG. 6. (a) Order parameters as a function of ϕ along the dashed line in Fig. 5. (b) Characteristic wave vectors Q_x and Q_y extracted from the structure factor $\mathcal{S}_x$ and $\mathcal{S}_y$. The SP-yz-FM-yz-AF phase transitions are indicated by the sudden change of order parameters and by the jump of $Q_{x(y)}$.

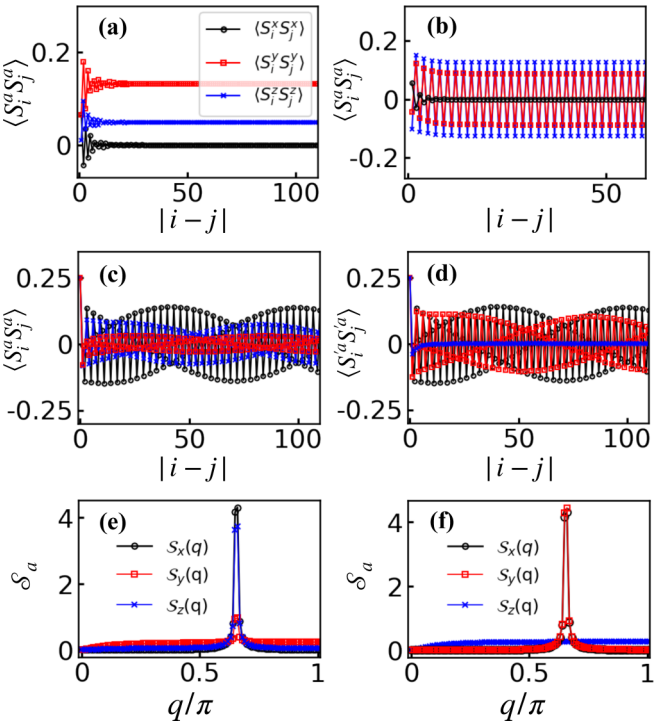

FIG. 7. Spin-spin correlation functions for the ground state of Eq. (13). (a) $\langle S_i^a S_j^a \rangle$ versus $|i-j|$ with $\phi = 0.35\pi$, showing long-range ferromagnetic correlations in $\hat{y}$ and $\hat{z}$ directions. (b) $\langle S_i^a S_j^a \rangle$ with $\phi = 0.45\pi$, showing long-range antiferromagnetic correlations. $\langle S_i^x S_j^x \rangle$ drops to zero rapidly. (c) Oscillatory correlation functions in the SP. The corresponding structure factors $\mathcal{S}_a$ as a function of wave vector q are depicted in (e). All three components exhibit a clear peak at $q \simeq 0.655\pi$. (d) The same as (c) but with S_i^a replaced by $S_i'^a$. The exponential decay of $\langle S_i'^z S_j'^z \rangle$ indicates that the spin spirals around the DM vector $\vec{D}$. (f) Structure factors for the data in (d).

magnetization, and staggered magnetization along $\hat{y}$ and $\hat{z}$. This result agrees with the variation of characteristic wave vectors Q_y and Q_z as a function of ϕ; see Fig. 6(b).

Spin correlation functions $\langle S_i^a S_j^a \rangle$, $a = x, y, z$ with representative parameters are depicted in Figs. 7(a)–7(c). Here we set $\alpha = 0.28\pi$. In the yz-FM [see Fig. 7(a) with $\phi = 0.35\pi$], there are long-range ferromagnetic correlations in $\hat{y}$ and $\hat{z}$ directions. In the yz-AF [see Fig. 7(b) with $\phi = 0.45\pi$], the correlations along $\hat{y}$ and $\hat{z}$ are ferromagnetic. In Fig. 7(c) we show the result for $\phi = 0.2\pi$ (in the SP). All correlation functions exhibit long-range oscillations. Their amplitudes are different due to the anisotropy in exchange terms. The spiral nature can be seen from $\mathcal{S}_a$ with local peaks at $Q_{x,y,z} \simeq 0.655\pi$, as shown in Fig. 7(e). Note that the energy for the DM term can be minimized by arranging the whirly spins in the plane perpendicular to $\vec{D}$. To show this, here we can define $S_j'^y = S_j^y \cos\gamma - S_j^z \sin\gamma$, $S_j'^z = S_j^y \sin\gamma + S_j^z \cos\gamma$ [$\gamma = \arctan(D_y/D_z)$] and $S_j'^x = S_j^x$. By substituting the correlation functions with $\langle S_i'^a S_j'^a \rangle$, as shown in Fig. 7(d), $\langle S_i'^x S_j'^x \rangle$ and $\langle S_i'^y S_j'^y \rangle$ oscillate in a similar pattern whereas $\langle S_i'^z S_j'^z \rangle$ decays rapidly to zero. The structure factor alters to $\mathcal{S}'^a(q) = \langle \sum_{i,j} e^{iq(i-j)} S_i'^a S_j'^a \rangle / L$, which is plotted in Fig. 7(f). Here $\mathcal{S}_z$ is flattened but $\mathcal{S}_x$ and $\mathcal{S}_x$ still share the same peak. This confirms

that $S_j'^z$ is now along the rotation axis $\vec{D}$, and $S_j'^{x,y}$ reveals the spiral feature as expected.

VI. SUMMARY

In summary, we have studied the effective spin models for 1D BHM with synthetic gauge fields in the strongly interacting limit. We have shown how an effective spin model can be derived through the method of adiabatic elimination. The effective Hamiltonian for a generalized BHM is obtained, showing the appearance of the DM interaction and the symmetric anisotropic coupling in an *XYZ* model. Typical cases either with or without magnetic flux are demonstrated. We have studied the phase diagram of the *XYZ* model with DM interaction and transverse field. In this case, four phases are identified: the *xy*-SP induced by the DM coupling along the $\hat{z}$ direction, the *y*-FM and *y*-AF as a result of dominant spin-spin coupling along $\hat{y}$, as well as the *x*-PM due to the presence of transverse field. With both SOCs and synthetic magnetic flux, we have also studied the interplay between the anisotropic coupling and the DM interaction with two components in $\vec{D}$. Three phases are identified, including a SP with spins spiraling in the plane perpendicular to $\vec{D}$, as well as *yz*-FM and *yz*-AF caused by the anisotropic coupling.

It is worth noting that by releasing the constraints on diagonal hoppings, multicomponents appear in the DM interaction and the symmetric anisotropic coupling, which may give rise to richer phases. On the other hand, the adiabatic elimination approach for effective Hamiltonian can be applied to Hubbard model in two and higher dimensions. The corresponding spin models are of further interest in studying intriguing magnetic textures and phases.

ACKNOWLEDGMENTS

This work is supported by NSFC (Grant No. 11804181), the National Key R&D Program of China (Grant No. 2018YFA0306504), the Research Fund Program of the State Key Laboratory of Low-Dimensional Quantum Physics (Grant No. ZZ201803), and the China Postdoctoral Science Foundation (Grant No. 2019M650025).

[1] C. Gross and I. Bloch, Science **357**, 995 (2017).
[2] F. Schafer, T. Fukuhara, S. Sugawa, Y. Takasu, and Y. Takahashi, Nat. Rev. Phys. **2**, 411 (2020).
[3] D. Jaksch, C. Bruder, J. I. Cirac, C. W. Gardiner, and P. Zoller, Phys. Rev. Lett. **81**, 3108 (1998).
[4] M. Lewenstein, A. Sanpera, and V. Ahufinger, *Ultracold Atoms in Optical Lattices: Simulating Quantum Many-Body Systems* (Oxford University Press, Oxford, UK, 2012).
[5] I. Bloch, J. Dalibard, and S. Nascimbene, Nat. Phys. **8**, 267 (2012).
[6] Y. Ohashi and A. Griffin, Phys. Rev. Lett. **89**, 130402 (2002).
[7] P. G. Kevrekidis, G. Theocharis, D. J. Frantzeskakis, and B. A. Malomed, Phys. Rev. Lett. **90**, 230401 (2003).
[8] M. Theis, G. Thalhammer, K. Winkler, M. Hellwig, G. Ruff, R. Grimm, and J. H. Denschlag, Phys. Rev. Lett. **93**, 123001 (2004).
[9] K. Sengupta and N. Dupuis, Phys. Rev. A **71**, 033629 (2005).
[10] M. Capello, F. Becca, M. Fabrizio, and S. Sorella, Phys. Rev. Lett. **99**, 056402 (2007).
[11] W. S. Bakr, A. Peng, M. E. Tai, R. Ma, J. Simon, J. I. Gillen, S. Foelling, L. Pollet, and M. Greiner, Science **329**, 547 (2010).
[12] M. Aidelsburger, M. Atala, M. Lohse, J. T. Barreiro, B. Paredes, and I. Bloch, Phys. Rev. Lett. **111**, 185301 (2013).
[13] H. Miyake, G. A. Siviloglou, C. J. Kennedy, W. C. Burton, and W. Ketterle, Phys. Rev. Lett. **111**, 185302 (2013).
[14] A. Celi, P. Massignan, J. Ruseckas, N. Goldman, I. B. Spielman, G. Juzeliūnas, and M. Lewenstein, Phys. Rev. Lett. **112**, 043001 (2014).
[15] B. Stuhl, H.-I. Lu, L. Aycock, D. Genkina, and I. Spielman, Science **349**, 1514 (2015).
[16] M. Mancini *et al.*, Science **349**, 1510 (2015).
[17] V. Galitski and I. B. Spielman, Nature (London) **494**, 49 (2013).
[18] M. Atala, M. Aidelsburger, M. Lohse, J. T. Barreiro, B. Paredes, and I. Bloch, Nat. Phys. **10**, 588 (2014).
[19] C. Hamner, Y. Zhang, M. A. Khamehchi, M. J. Davis, and P. Engels, Phys. Rev. Lett. **114**, 070401 (2015).
[20] H. Zhai, Rep. Prog. Phys. **78**, 026001 (2015).
[21] Z. Wu, L. Zhang, W. Sun, X.-T. Xu, B.-Z. Wang, S.-C. Ji, Y. Deng, S. Chen, X.-J. Liu, and J.-W. Pan, Science **354**, 83 (2016).
[22] F. A. An, E. J. Meier, and B. Gadway, Sci. Adv. **3**, e1602685 (2017).
[23] L.-M. Duan, E. Demler, and M. D. Lukin, Phys. Rev. Lett. **91**, 090402 (2003).
[24] A. B. Kuklov and B. V. Svistunov, Phys. Rev. Lett. **90**, 100401 (2003).
[25] E. Altman, W. Hofstetter, E. Demler, and M. D. Lukin, New J. Phys. **5**, 113 (2003).
[26] I. Dzyaloshinsky, J. Phys. Chem. Solids **4**, 241 (1958).
[27] T. Moriya, Phys. Rev. **120**, 91 (1960).
[28] W. S. Cole, S. Zhang, A. Paramekanti, and N. Trivedi, Phys. Rev. Lett. **109**, 085302 (2012).
[29] J. Radić, A. Di Ciolo, K. Sun, and V. Galitski, Phys. Rev. Lett. **109**, 085303 (2012).
[30] M. Gong, Y. Qian, M. Yan, V. Scarola, and C. Zhang, Sci. Rep. **5**, 10050 (2015).
[31] Z. Xu, W. S. Cole, and S. Zhang, Phys. Rev. A **89**, 051604(R) (2014).
[32] M. Piraud, Z. Cai, I. P. McCulloch, and U. Schollwöck, Phys. Rev. A **89**, 063618 (2014).
[33] L. Zhang, Y. Ke, and C. Lee, Phys. Rev. B **100**, 224420 (2019).
[34] D. Coffey, T. M. Rice, and F. C. Zhang, Phys. Rev. B **44**, 10112 (1991).
[35] R. Jafari, M. Kargarian, A. Langari, and M. Siahatgar, Phys. Rev. B **78**, 214414 (2008).
[36] R. Jafari and A. Langari, arXiv:0812.1862.
[37] B.-Q. Liu, B. Shao, J.-G. Li, J. Zou, and L.-A. Wu, Phys. Rev. A **83**, 052112 (2011).
[38] M. Soltani, J. Vahedi, M. Abolhassani, and A. Masoudi, ISRN Condens. Matter Phys. **2011**, 980192 (2011).
[39] S. Peotta, L. Mazza, E. Vicari, M. Polini, R. Fazio, and D. Rossini, J. Stat. Mech. (2014) P09005.

[40] H. T. Nembach, J. M. Shaw, M. Weiler, E. Jué, and T. J. Silva, Nat. Phys. **11**, 825 (2015).
[41] K. Di, V. L. Zhang, H. S. Lim, S. C. Ng, M. H. Kuok, J. Yu, J. Yoon, X. Qiu, and H. Yang, Phys. Rev. Lett. **114**, 047201 (2015).
[42] J. Zhao, S. Hu, J. Chang, F. Zheng, P. Zhang, and X. Wang, Phys. Rev. B **90**, 085117 (2014).
[43] F. Mila and K. P. Schmidt, *Strong-Coupling Expansion and Effective Hamiltonians* (Springer, Berlin, Heidelberg, 2011).
[44] M. Bukov, M. Kolodrubetz, and A. Polkovnikov, Phys. Rev. Lett. **116**, 125301 (2016).
[45] E. Brion, L. H. Pedersen, and K. Mølmer, J. Phys. A: Math. Theor. **40**, 1033 (2007).
[46] M. Sanz, E. Solano, and Í. L. Egusquiza, *Beyond Adiabatic Elimination: Effective Hamiltonians and Singular Perturbation* (Springer, Tokyo, 2016).
[47] I. L. Egusquiza, arXiv:1309.0628.
[48] J. P. Killingbeck and G. Jolicard, J. Phys. A: Math. Gen. **36**, R105 (2003).
[49] A. Meurer *et al.*, PeerJ Comput. Sci. **3**, e103 (2017).
[50] M. Brockmann, A. Klümper, and V. Ohanyan, Phys. Rev. B **87**, 054407 (2013).
[51] X. Li, E. Zhao, and W. V. Liu, Nat. Commun. **4**, 1523 (2013).
[52] H. Alaeian, C. W. S. Chang, M. V. Moghaddam, C. M. Wilson, E. Solano, and E. Rico, Phys. Rev. A **99**, 053834 (2019).
[53] J. H. Kang, J. H. Han, and Y. Shin, New J. Phys. **22**, 013023 (2020).
[54] J. G. Rau, E. K.-H. Lee, and H.-Y. Kee, Phys. Rev. Lett. **112**, 077204 (2014).
[55] G. Vidal, Phys. Rev. Lett. **98**, 070201 (2007).
[56] F. Verstraete, V. Murg, and J. I. Cirac, Adv. Phys. **57**, 143 (2008).
[57] R. Orús, Ann. Phys. **349**, 117 (2014).
[58] U. Schollwöck, J. Richter, D. Farnell, and R. Bishop, *Quantum Magnetism* (Springer, Berlin, Heidelberg, 2004).
[59] M. A. Cazalilla, R. Citro, T. Giamarchi, E. Orignac, and M. Rigol, Rev. Mod. Phys. **83**, 1405 (2011).
[60] A. Langari, Phys. Rev. B **69**, 100402(R) (2004).
[61] I. P. McCulloch, J. Stat. Mech. (2007) P10014.
[62] U. Schollwöck, Ann. Phys. **326**, 96 (2011).